DECEMBER 14 2009

Transmission characteristics of a tee-junction in a rectangular duct at higher-order modes

Siu-Kit Lau; Kwan-Hao Leung

J. Acoust. Soc. Am. 126, 3028–3039 (2009)
https://doi.org/10.1121/1.3257209

Transmission characteristics of a tee-junction in a rectangular duct at higher-order modes

Siu-Kit Lau[a)]
Architectural Engineering Program, University of Nebraska-Lincoln, 1110 South 67th Street, Omaha, Nebraska 68182-0681

Kwan-Hao Leung[b)]
Department of Building Services Engineering, The Hong Kong Polytechnic University, Hung Hom, Hong Kong, People's Republic of China

(Received 20 February 2009; revised 1 September 2009; accepted 29 September 2009)

Numerical and experimental studies were undertaken to characterize the noise transmission and scattering properties in higher-order modes across the tee-junction of a rectangular duct used in ventilation and air-conditioning systems. To measure these properties, a formulation of a transmission matrix based on the transfer function and a two-microphone method was devised. The measurement of modal sound transmission and scattering coefficients is demonstrated for a duct element in a rectangular duct. The results of numerical simulations were verified by experiments. The results show that sound transmissions of fundamental mode and higher-order modes across the main duct are high at the eigen-frequencies of the main duct and sidebranch. Weak modal coupling of the branch-modes and the traveling wave in the main duct is observed at or very close to the eigen-frequencies of the sidebranch, which shifts excitation of the higher-order branch-modes at higher frequencies. A decrease in sound transmission and increase in sound scattering into higher-order modes occur with excitation of the axial branch-mode. Excitation of the longitudinal branch-mode due to branch-end reflection also results in lower sound transmission of higher-order modes across the junction along the main duct.
 [DOI: 10.1121/1.3257209]

PACS number(s): 43.55.Rg, 43.20.Mv [SFW] Pages: 3028–3039

I. INTRODUCTION

Sound propagation in duct systems is well known as an important problem in building, automotive, and aeronautic noise control. Duct systems consist of a network of various elements (e.g., bends and constrictions) in addition to straight sections. Such elements of duct systems (other than straight ducts) alter the acoustic impedance and thus causes the reflection of sound in the system.

In recent decades, the sound-transmission characteristics of some duct elements have been investigated at low frequency, including bends,[1] sidebranches,[2,3] constrictions,[4] and expansions;[5] however, textbooks on engineering design (e.g., Refs. 6 and 7) typically contain few predictions of sound-transmission loss at very low frequency for these conventional passive duct elements. Inaccurate estimates of sound-transmission loss arise when the frequency is close to and higher than the first cut-on frequency of the duct. The effective control of such noise in ducts would require a comprehensive characterization and specific measurement procedure for sound transmission and scattering across duct elements in higher-order modes.

Sidebranches are one of the most common elements in duct networks, commonly used for flow separation when coupled with straight ducts and other elements. Tang and Li[2] undertook theoretical and experimental studies of the sound-transmission loss of double sidebranches using plane-wave theory and the two-microphone method, respectively. The authors found that predictions based on plane-wave theory are only accurate when the sidebranch is distant from other duct elements or when the original sound-transmission loss of other duct elements is weak. Moreover, the sound excitation of axial branch-modes yields lower sound transmission across a tee-junction located along the main duct.[3] However, the studies are limited to the sound-transmission fundamental mode below the first eigen-frequency of the main duct.

For measurement of the sound reflection and transmission coefficients of a duct element, Parrondo *et al.*[8] extended the two-microphone method for measurement of the transmission and reflection matrix of a sidebranch, using three loudspeakers and six sound-pressure microphones. The investigations of the sound transmission of a sidebranch are again limited to analyses of propagation of fundamental mode along the main duct. In addition, use of the two-microphone method in experimental studies is restricted to low frequencies (i.e., below the first eigen-frequency of the duct) because of the fundamental-mode (plane wave) assumption; however, sound propagation at higher-order modes is also important for noise control, especially in the case of large ducts. For example, the typical dimension (i.e., width and/or height) of air-conditioning ducts is up to about 3 m,[9] which corresponds to a low first cut-on frequency of

[a)]Author to whom correspondence should be addressed. Electronic mail: slau3@unl.edu
[b)]Present address: Ove Arup & Partners Hong Kong Ltd., L5 Festival Walk, 80 Tat Chee Avenue, Kowloon Tong, Kowloon, Hong Kong.

the duct (57 Hz). In such cases, sound propagation in higher-order modes becomes of greater practical importance in terms of noise control.

A theoretical solution for a tee-junction has been formulated using the Fourier transform and a mode matching technique;[10,11] however, there exist few case studies of such problems. The interaction of acoustic modes and the transmission and scattering of sound across a tee-junction in the duct has yet to be clearly addressed. It is therefore worthwhile to study the sound-transmission characteristics of a tee-junction and to conduct a more in-depth analysis of the problem for higher-order modes.

In the measurement of sound propagation in higher-order duct modes, the assumptions involved in the two-microphone method are invalid and the complexity of the measurement is increased compared with that for fundamental mode. A modal decomposition method has been suggested to overcome these problems.[12] Abom[13] proposed a direct method based on the measurement of transfer functions between the microphone pairs in order to separate the modes in a duct section into incident and reflected parts. To perform a modal decomposition of N number of modes requires the incident and reflected wave of each mode to be determined, as well as measurement of the sound pressures at $2\times N$ independent spatial locations with N independent source conditions. For circular ducts, this method can extend the measurement to frequencies below the first cut-on frequency of the radial mode when ten measurement positions are used (i.e., separation of the first five modes). A reduction in the number of measurement locations can be offset by measurements undertaken with different load conditions[14] at sites located downstream of the duct element. Previous works have generally considered circular ducts. Schultz *et al.*[15] determined the reflection and modal scattering coefficients of acoustic liners using the direct method in a square duct; however, few studies have applied the modal decomposition method to rectangular ducts and their elements.[16]

The aim of the present paper is to investigate and characterize sound propagation in higher-order modes across a tee-junction within a rectangular duct, using numerical (finite element method) and experimental (direct modal decomposition method) approaches. The resultant transmission matrix of a tee-junction is experimentally verified using the modal decomposition technique. We demonstrate a measurement procedure for sound transmission and the scattering coefficients of rectangular duct elements, which can be applied under the propagation conditions of higher-order modes. Also discussed are practical difficulties involved in measuring the transmission matrix of duct elements. The present study extends the work of Tang[3] to higher-order modes. It is hoped that the results will provide a more complete picture of the acoustical properties of tee-junctions (particularly for the air duct used in the ventilation and air-conditioning), thereby providing improved duct noise control and a useful experimental approach for investigating sound transmission and scattering within duct elements at higher-order modes.

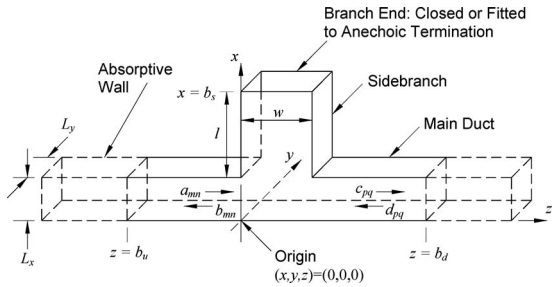

FIG. 1. Schematic diagram of sound transmission within a duct across a tee-junction, showing the employed coordinate system.

II. COMPUTATIONAL MODEL AND EXPERIMENTAL METHOD

Numerical and experimental studies were undertaken to characterize the sound transmission and scattering properties in higher-order modes across the tee-junction of a rectangular duct commonly used in ventilation and air-conditioning system. The methodologies are discussed in Secs. II A and II B, respectively.

A. Computational domain

Consider a tee-junction in a rectangular duct consisting of acoustically hard surfaces (see Fig. 1). All dimensions are normalized by the duct width L_x. The origin of the coordinate system is set at the left-side entry to the tee-junction. The width w and length l of the sidebranch can be varied relative to L_x. For simplicity, a two-dimensional system is considered in the numerical experiment. Axial modes in the axis along the sidebranch are considered. Some effects of spanwise modes along the y-axis of a three-dimensional system will be discussed later in the experimental investigation. A finite element computation is used to solve the inhomogeneous wave equation, given as

$$\nabla^2\hat{p} + k^2\hat{p} = \hat{q}, \tag{1}$$

where $\hat{p}$ and k are the acoustic pressure and the wavenumber of the sound, respectively; $\hat{q}$ denotes the source strength density of the excitation; and ∇^2 is the Laplacian operator over a specified domain with Neumann boundary conditions. The partial differential equation (PDE) solver within the software MATLAB was used to solve Eq. (1) in the present numerical experiments. The "assempde" of MATLAB function is used. The side walls of the duct and the sidebranch are acoustically rigid; therefore, the normal pressure gradient vanishes and the boundary condition is

$$\left.\frac{\partial\hat{p}}{\partial\hat{n}}\right|_{\text{wall}} = 0, \tag{2}$$

where $\hat{n}$ is the outward unit normal to the boundary. The main duct consists of two anechoic terminations at $z<-10L_x$ and $z>(10L_x+w)$. The higher-order modes are present in the main duct and sidebranch at frequencies above the first eigen-frequencies of the main duct and sidebranch, respectively. To damp down the higher-order modes before they reach the end boundaries, we adopt the impedance-matched anechoic termination of Tang and Lau,[4] whose

walls are acoustically absorptive. The boundary conditions of the absorptive side walls are given as

$$\frac{\partial \hat{p}}{\partial \hat{n}} \pm jk\gamma\hat{p} = 0, \tag{3}$$

where $j=\sqrt{-1}$. γ denotes an artificial absorption coefficient that is set at $0.01(z+b_u)^2$ and $0.01(z-b_d)^2$ for the upstream and downstream absorptive endings of the main duct, respectively, as in Ref. 3. $b_u=-10L_x$ and $b_d=(10L_x+w)$. A termination length greater than $10L_x$ is used in the analysis. The boundary condition at the exit of an anechoic termination is set as described in Eq. (3), with $\gamma=1$ for an outgoing wave. Two types of sidebranch endings are considered: infinitely long and closed sidebranches. They are tested for two situations of weak and strong branch-end reflections. For an infinitely long sidebranch, the anechoic termination is set at $x>b_s$ with $\gamma=0.01(x-b_s)^2$, where $b_s=L_x+l$. Although the acoustic properties are independent of sidebranch length in the case of an infinitely long sidebranch, the length is set to $l=5L_x$. For a closed sidebranch, the boundary condition described in Eq. (2) is set at $x=b_s$, $\forall z\in[0,w]$.

Upstream of the duct ($z<0$), an incident field a_{mn} propagates toward the tee-junction, as shown in Fig. 1. In the present study, the excitation of this incident field is applied at $z=b_u$. Sound is investigated at frequencies below the first symmetric duct mode ($m=2$ and $p=2$) of the x-axis in the main duct (i.e., $kL_x=2\pi$). For investigations of the higher-order-mode propagation, two types of excitation are considered:

$$\hat{q} = 2jk\delta(z-b_u) \quad \text{Excitation Type 1: } \forall\, x\in[0,L_x], \tag{4a}$$

$$\hat{q} = 2jk\delta(z-b_u) \quad \text{Excitation Type 2: } \forall\, x\in[0,0.5L_x], \tag{4b}$$

where δ denotes a delta function. The former (Excitation Type 1) refers to fundamental-mode (unit plane wave) excitation, while the latter (Excitation Type 2) is asymmetric wave excitation and the source is bounded at $x\in[0,0.5L_x]$. The modal amplitudes arising from Type 2 excitations can be found using the wave equation.[16] Both the fundamental mode and first mode are excited by asymmetric wave excitation in Eq. (4b) at frequencies of $\pi\leq kL_x<2\pi$. The resultant sound-pressure field of the fundamental mode and higher-order modes at either side of the junction and without the junction can be decomposed by the method of modal decomposition.[17] The resultant sound-pressure fields due to excitation of the first mode only can be found by subtracting the contribution of the unit plane-wave excitation with the scattering coefficients, as calculated using Eq. (4a).

B. Experimental methodology

At any location (x,y,z) within the duct upstream of the junction ($b_u<z<0$) in Fig. 1, the general solution of acoustic pressure to the inhomogeneous Helmholtz equation described in Eq. (1) in a three-dimensional system at driving frequency ω and time t can be written as

$$\hat{p}(x,y,z)e^{j\omega t} = \sum_{m,n=0}^{\infty} \psi_{m,n}(x,y)[a_{mn}e^{j(\omega t-k_{z,mn}z)} + b_{mn}e^{j(\omega t+k_{z,mn}z)}], \tag{5}$$

where $\psi_{m,n}(x,y)$ are the eigen-functions of the acoustic modal pressure distribution inside the duct. The integers m and n are the acoustic duct mode numbers of the x-axis and y-axis, respectively, upstream of the junction in the main duct, which $(m,n)=(0,0)$ denotes fundamental mode and others denote higher-order modes. The duct has a rectangular cross-section of dimension L_x by L_y. $k_{z,mn}$ is the wavenumber of the duct mode in the axial direction,[18] where

$$k_{z,mn}^2 = k^2 - k_{mn}^2, \tag{6}$$

and

$$k_{mn}^2 = \left(\frac{m\pi}{L_x}\right)^2 + \left(\frac{n\pi}{L_y}\right)^2. \tag{7}$$

a_{mn} and b_{mn} are the complex acoustic pressure modal amplitudes of the traveling waves of (m,n) mode toward the junction (incident wave) and in the upstream part (reflected wave) of the main duct, respectively, as shown in Fig. 1. To decompose the incident and reflected sound-pressure fields (a_{mn} and b_{mn}, respectively), the microphones should be located with some transverse and axial separation in the area upstream of the junction.

A simple approach is to divide the microphones into two groups separated by an axial distance, u. For the decomposition of N number of modes, at least N microphones at each group are placed on the same axial location. Therefore, $2\times N$ microphones are used on each side of the tee-junction along the main duct. In the matrix form of Eq. (5), a vector of sound pressures at the same axial location z and η number of independent transverse locations inside the duct can be written simply as the product of the acoustic mode shape matrix at points $\mathbf{\Phi}$, the propagating mode matrix $\mathbf{Z}$, and the complex acoustic pressure modal amplitude vectors of incident and reflected waves ($\mathbf{a}$ and $\mathbf{b}$, respectively) due to the following sources:

$$\hat{\mathbf{p}} = \begin{bmatrix} \hat{p}(x_1,y_1,z) \\ \hat{p}(x_2,y_2,z) \\ \vdots \\ \hat{p}(x_\eta,y_\eta,z) \end{bmatrix} = \mathbf{\Phi}^T\mathbf{Z}\mathbf{a} + \mathbf{\Phi}^T\mathbf{Z}^{-1}\mathbf{b}, \tag{8}$$

where

$$\mathbf{\Phi} = \begin{bmatrix} \psi_{0,0}(x_1,y_1) & \psi_{0,0}(x_2,y_2) & \cdots & \psi_{0,0}(x_\eta,y_\eta) \\ \psi_{1,0}(x_1,y_1) & \psi_{1,0}(x_2,y_2) & \cdots & \psi_{1,0}(x_\eta,y_\eta) \\ \vdots & \vdots & \ddots & \vdots \\ \psi_{m,n}(x_1,y_1) & \psi_{m,n}(x_2,y_2) & \cdots & \psi_{m,n}(x_\eta,y_\eta) \end{bmatrix},$$

and $\mathbf{Z}=\mathrm{diag}(e^{-jk_{z,00}z},\ e^{-jk_{z,10}z},\cdots e^{-jk_{z,mn}z})$ is a diagonal matrix. The superscript T denotes matrix transpose. To solve the incident and reflected waves, additional vectors of sound pressures are required with σ number of linear independent source conditions to form a matrix such that

$$\hat{\mathbf{p}} = \mathbf{\Phi}^T \mathbf{Z} \mathbf{A} + \mathbf{\Phi}^T \mathbf{Z}^{-1} \mathbf{B}, \tag{9}$$

where **A** and **B** are $[\{\mathbf{a}\}_1\{\mathbf{a}\}_2 \ldots \{\mathbf{a}\}_\sigma]$ and $[\{\mathbf{b}\}_1\{\mathbf{b}\}_2 \ldots \{\mathbf{b}\}_\sigma]$, respectively. $\{\mathbf{a}\}_i$ and $\{\mathbf{b}\}_i$ are the complex acoustic pressure modal amplitude vectors of incident and reflected waves, respectively, due to ith source condition. $\hat{\mathbf{p}} = [\{\hat{\mathbf{p}}\}_1\{\hat{\mathbf{p}}\}_2 \cdots \{\hat{\mathbf{p}}\}_\sigma]$. The transfer matrix, $\mathbf{H_{ab}}$, of the two groups of microphones upstream of the junction at $z = z_a$ and z_b, respectively, is defined as

$$\mathbf{H_{ab}} \hat{\mathbf{p}}_\mathbf{a} = \hat{\mathbf{p}}_\mathbf{b}, \tag{10}$$

where the subscripts **a** and **b** denote the quantities associated with the axial location at z_a and z_b, respectively, in the upstream with an axial separation of $z_b - z_a = u$. Substituting Eq. (9) into Eq. (10), we find that the reflection matrix of the junction (or other duct elements) can be estimated from experimental data as

$$\mathbf{B} \mathbf{A}^{-1} = \mathbf{Z_a} \mathbf{R_{ab}} \mathbf{Z_a}, \tag{11}$$

where

$$\mathbf{R_{ab}} = (\mathbf{\Phi}_\mathbf{b}^T \mathbf{Z}_\mathbf{u}^{-1} - \mathbf{H_{ab}} \mathbf{\Phi}_\mathbf{a}^\mathbf{T})^{-1} (\mathbf{H_{ab}} \mathbf{\Phi}_\mathbf{a}^T - \mathbf{\Phi}_\mathbf{b}^T \mathbf{Z_u}), \tag{12}$$

and

$$\mathbf{Z_u} = \mathrm{diag}\left(e^{-jk_{z,00}(z_b - z_a)}, \quad e^{-jk_{z,10}(z_b - z_a)}, \quad \ldots, \quad e^{-jk_{z,mn}(z_b - z_a)}\right). \tag{13}$$

The amplitude of the diagonal elements in the diagonal matrix $\mathbf{Z_a}$ is unity; therefore, the modal sound-power reflection coefficients upstream of the tee-junction can be found from the values of the elements of $\mathbf{R_{ab}}$ in Eq. (12). Substituting Eq. (11) into Eq. (9), the sound pressures at $z = z_a$ can be rewritten as

$$\hat{\mathbf{p}}_\mathbf{a} = \mathbf{\Phi}_\mathbf{a}^T (\mathbf{I} + \mathbf{R_{ab}}) \mathbf{Z_a} \mathbf{A}. \tag{14}$$

To solve the incident and reflected sound-pressure fields downstream of the main duct, suppose there are two other groups of microphones downstream of the tee-junction at axial locations of z_c and z_d of the main duct, respectively. Equations (8)–(13) can then be applied. The sound pressure at $z = z_c$ can be found as

$$\hat{\mathbf{p}}_\mathbf{c} = \mathbf{\Phi}_\mathbf{c}^T (\mathbf{I} + \mathbf{R_{cd}}) \mathbf{Z_c} \mathbf{C}, \tag{15}$$

I is the unit matrix. **C** denotes the modal amplitude matrix of complex acoustic pressure of wave transmitted downstream with σ number of linear independent source conditions, which consists of a complex acoustic pressure amplitude c_{pq} of (p,q) mode. The integers p and q are the acoustic duct mode numbers of the x-axis and y-axis, respectively, downstream of the junction in the main duct. $\mathbf{R_{cd}}$ is the modal amplitude matrix of the reflection coefficients of the ending downstream (right-hand end) of the duct, which can be found by Eq. (12) with subscripts **c** and **d** instead of **a** and **b**, respectively. By Eq. (14) and (15), the transmission matrix of the junction can be written as

$$\mathbf{C} \mathbf{A}^{-1} = \mathbf{Z_c}^{-1} \mathbf{T} \mathbf{Z_a}, \tag{16}$$

TABLE I. Eigen-frequencies, k_{mn}, of the duct normalized by the first eigen-frequency, $k_{mn=(1,0)}$.

Acoustic modes (m,n)	$k_{mn}/k_{mn=(1,0)}$
(1,0)	1.00
(0,1)	1.15
(1,1)	1.53
(2,0)	2.00

$$\mathbf{T} = [\mathbf{\Phi}_\mathbf{c}^T (\mathbf{I} + \mathbf{R_{cd}})]^{-1} \mathbf{H_{ac}} [\mathbf{\Phi}_\mathbf{a}^T (\mathbf{I} + \mathbf{R_{ab}})], \tag{17}$$

where the subscripts **c** and **d** denote the quantities associated with the axial locations at z_c and z_d, respectively, of the main duct and the area downstream of the junction. $\mathbf{H_{ac}} = \hat{\mathbf{p}}_\mathbf{c} \hat{\mathbf{p}}_\mathbf{a}^{-1}$ is the transfer matrix of sound-pressure groups located at z_a and z_c.

Equation (16) can be further simplified by removing a microphone layer when an anechoic termination is installed at the downstream ending where $\mathbf{R_{cd}} = 0$ or when a termination with specified modal reflection is installed. For a modal decomposition of N number of modes, measurements should be carried out with at least $N = \eta$ and $N = \sigma$. The solution of the over-determined case can be found with $N < \eta$. **T** is the modal complex amplitude matrix of the transmission coefficient. This matrix is independent of upstream conditions, which consist of N^2 coefficients:

$$T_{mn,pq}, \quad m,n,p,q = 1,2, \ldots, N,$$

representing the sound transmission or scattering coefficient amplitude from the (m,n) mode upstream of the junction in the main duct to the (p,q) mode downstream of the junction. The forms of Eqs. (12) and (17) are similar to those of the well-known two-microphone method for fundamental mode.

An experiment was performed to verify and extend the results of the numerical investigation. A test rig was constructed in which the main duct used in the measurements in Fig. 1 was made of 20-mm-thick Perspex with a rectangular cross-section of dimensions $L_x = 173$ mm and $L_y = 150$ mm. This set-up yielded a first eigen-frequency of 991 Hz in the main duct. Table I shows the normalized eigen-frequencies of the first four modes of the main duct. The sidebranch has the same cross-sectional dimensions as the main duct, with a sidebranch length l of 1 m. The end of the sidebranch can be closed or fitted with an anechoic termination. A loudspeaker was mounted at one end of the main duct; the other end was terminated anechoically using a length of highly absorbent duct end, as described in Ref. 2, to eliminate the reflection of sound produced at the other end of the main duct. The sound-power reflection coefficient was less than 0.6% at the frequency of interest, indicating that an anechoic condition was establish.

To resolve sound transmission and scattering of the first four modes, four microphones are required at each of four axial locations (i.e., 16 microphones in total). The microphones were flush mounted in the sides of the duct. The number and locations of the microphones were chosen to observe the desired acoustic modes, which are the (0,0), (1,0), (0,1), and (1,1) modes. The locations of microphones are listed in Table II. The measurement microphones were

TABLE II. Locations of microphones within the duct (mm).

Microphone No.	Transverse location (x,y)	Axial location, z
1	(153, 0)	−670
2	(0, 20)	
3	(173, 130)	
4	(20, 150)	
5	(20, 0)	−620
6	(0, 130)	
7	(173, 20)	
8	(153, 150)	
9	(153, 0)	600
10	(0, 20)	
11	(173, 130)	
12	(20, 150)	
13	(20, 0)	650
14	(0, 130)	
15	(173, 20)	
16	(153, 150)	

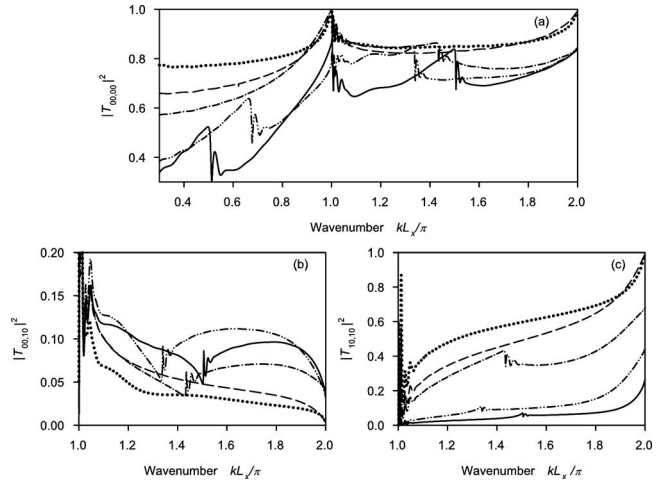

FIG. 2. Sound-power transmission and scattering across an infinitely long sidebranch along the main duct.(a) $|T_{00,00}|^2$, (b) $|T_{00,10}|^2$, and (c) $|T_{10,10}|^2$. (····) w/L_x=0.3; (– – – –) w/L_x=0.5; (–·–·–) w/L_x=0.7; (–··–··–) w/L_x=1.5; (—) w/L_x=2.0.

Bruel & Kjaer (B&K) Type 4935 microphones (7 mm diameter). For calibration of the amplitude and phase of all channels, each microphone was mounted in an intensity coupler (B&K Type 3541) with a reference microphone. The same acoustic pressure was exposed to the microphones, as only the fundamental mode could propagate inside the intensity coupler. The transfer functions of microphones were measured using a white noise generator (B&K Type ZI 0055) and then used to correct the response of each microphone. The phase mis-match among the microphones was less than ±2.7° at frequencies below 2 kHz. For the source conditions employed in measuring the higher-order modes, four independent source conditions were generated with four different restrictor plates, as described in Schultz *et al.*[15]

III. RESULTS AND DISCUSSION

A. Numerical investigation

As mentioned above, we investigated sound-wave propagation up to the eigen-frequency of the second x-axis mode (m=2 and p=2) at $kL_x=2\pi$ in the main duct. A two-dimensional system is considered in this section (n=0 and q=0). The sound transmission and scattering coefficients are estimated from the computed data at $[(z-w)/L_x]=8$ in order to eliminate the influence of evanescent waves. The numerical experiment focuses on the sound transmission and scattering of the fundamental mode (m=0) and first asymmetric mode (m=1) across a tee-junction along the main duct.

1. Infinitely long sidebranch

a. Sound-power transmission of the fundamental mode (0,0) at higher frequency, $|T_{00,00}|^2$. For an infinitely long sidebranch, the tee-junction is known to be a high-pass filter at frequencies below the first eigen-frequency of the main duct, $k_{mn=(1,0)}=\pi/L_x$.[3] Figure 2(a) shows the effects of w/L_x on the sound-power transmission of a fundamental mode $|T_{00,00}|^2$ across the junction along the main duct at higher frequencies below the eigen-frequencies of the (2,0) modes $[k \le k_{mn=(2,0)}]$. $|T_{00,00}|^2$ denotes the sound-power transmission-coefficient from fundament mode upstream of the junction $(m,n)=(0,0)$ to fundamental mode downstream of the junction $(p,q)=(0,0)$ in the main duct. A slight fluctuation in $|T_{00,00}|^2$ can be observed at frequencies just above $k_{mn=(1,0)}$, which can be caused by the strong evanescent waves close to the eigen-frequencies. At frequencies below the first eigen-frequency of the sidebranch, $k<\pi/w$, only a fundamental mode can propagate in the sidebranch. The peaks in $|T_{00,00}|^2$ occur at the eigen-frequencies of the x-axis modes in the main duct, $k_{mn=(m,0)}$, as shown in Fig. 2(a) with w/L_x=0.3 and 0.5, where it approaches unity at $kL_x=\pi$ and 2π. This indicates strong sound transmission of fundamental mode at the eigen-frequencies of axial mode in x-axis at the main duct. $|T_{00,00}|^2$ declines gradually and reaches a minimum at frequencies between two eigen-frequencies of x-axis modes in the main duct. The present study was extended to higher frequencies, and the same observations were found at other higher-order modes (data not shown).

A greater amount of acoustic power is transmitted into the sidebranch with increasing w/L_x by branch sound-power division,[19] resulting in a rapid decline in $|T_{00,00}|^2$ as the frequency increases from $k=k_{mn=(1,0)}=\pi/L_x$ and a lowering in the minimum point between $k_{mn=(m,0)}$, as shown in Fig. 2(a) with w/L_x=0.5 (cf. w/L_x=0.3). For large w/L_x, the nonplanar branch-mode, which is the higher-order axial mode of the side branch in the axis along the main duct z-axis, can be excited at a frequency of $k>\pi/w$; however, a local maximum of $|T_{00,00}|^2$ can be found at or very close to the eigen-frequencies of the sidebranch, $k=\alpha\pi/w$, where α is the axial branch-mode number for the z-axis.

An example with w/L_x=0.7 is shown in Fig. 2(a), where a local maximum in $|T_{00,00}|^2$ can be observed at the frequency of the first asymmetric branch-mode, $kL_x=1.429\pi$. For frequencies just above the eigen-frequencies of the sidebranch, we find a sharp fall in $|T_{00,00}|^2$ followed by fluctuating values. Subsequently, the trend resumes, increasing as the frequency approaches another higher eigen-frequency of an x-axis mode in the main duct; however, the peak of

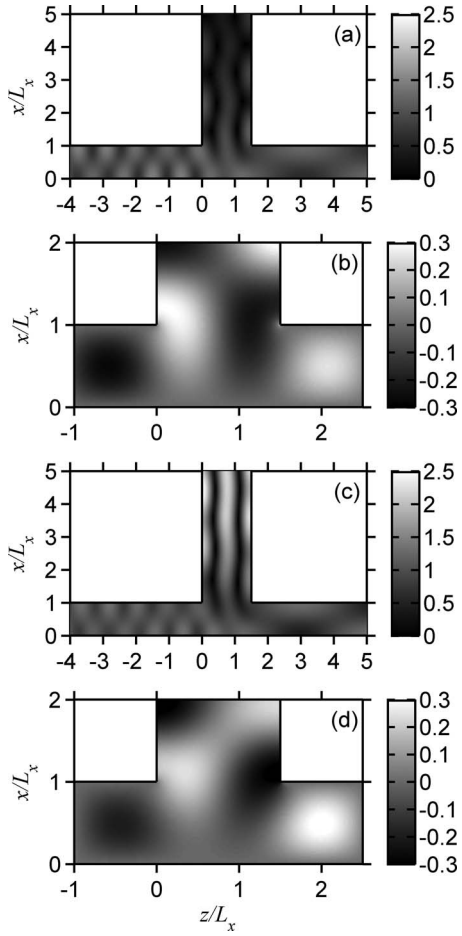

FIG. 3. Sound field around the tee-junction between the main duct and an infinitely long sidebranch with $w/L_x=1.5$ due to fundamental-mode excitation. (a) $kL_x=1.333\pi$, pressure magnitude (Pa); (b) $kL_x=1.333\pi$, particle-velocity profile (toward the sidebranch), $\rho c v_x$(kg m^{-1} s^{-2}); (c) $kL_x=1.340\pi$, pressure magnitude (Pa); (d) $kL_x=1.340\pi$, particle-velocity profile (toward the sidebranch), $\rho c v_x$(kg m^{-1} s^{-2}). ρ, c, and v_x are the density of the media (kg/m^3), speed of sound in the media (m/s), and acoustic particle velocity (m/s), respectively.

$|T_{00,00}|^2$ at the eigen-frequencies of the main duct declines when the non-planar branch-mode is excited, as shown in Fig. 2(a) with $w/L_x=0.7$, 1.5, and 2.0 (cf. $w/L_x=0.3$ and 0.5). Similar patterns are found for higher branch-modes, e.g., Fig. 2(a) with $w/L_x=1.5$ and 2.0. The local maxima in $|T_{00,00}|^2$ are also found at or close to the eigen-frequency of the second branch-mode, $k=2L_x/w$. These maxima and subsequent fall at higher-order mode will now be discussed with the visualization of the sound pressure and particle-velocity fields in the rest of this sub-section.

Figure 3(a) shows the sound-pressure field at the eigen-frequency of the second branch-mode, $k=2L_x/w$, with $w/L_x=1.5$, due to fundamental-mode excitation. Higher sound pressure can be observed inside the junction at $x=0$. The distribution of acoustic velocity in x-axis toward the sidebranch, v_x (m/s), is asymmetric [Fig. 3(b)]; consequently, the symmetric branch-mode is suppressed at $kL_x=1.333\pi$. This mismatch results in increased $|T_{00,00}|^2$ in the main duct at and very close to the eigen-frequencies of the sidebranch [see Fig. 2(a)]. The situation is markedly different at frequencies slightly above the eigen-frequencies of the sidebranch, as shown in Fig. 3(c). This change occurs because the wavelength is slightly smaller than the width of the sidebranch at the frequencies immediately above the eigen-frequency of the sidebranch. This leads to an extension in the distribution of acoustic velocity in axis, v_x (m/s), toward the sidebranch at $x=L_x$ [Fig. 3(d)] and thus more effective excitation of the symmetric branch-mode. Strong resonance of the higher branch-mode is evident in Fig. 3(c). As a result of the large amount of acoustic power taken away by the strong resonance of the branch-mode, a slump occurs in the sound transmission $|T_{00,00}|^2$ across the junction along the main duct at frequencies slightly above the eigen-frequency of the sidebranch [see Fig. 2(a)].

The results also confirm that higher-order branch-mode excitation is shifted at higher frequency by the relatively uniform particle-velocity field toward the sidebranch, as evident in the results of Tang,[3] although this previous study did not explicitly specify the effects of the higher-order branch-mode. The present results indicate weak coupling of the traveling wave in the main duct and branch-modes at or very close to the eigen-frequencies of the sidebranch. This weak coupling arises because of the mismatch between the particle-velocity field and branch-mode at the entry to the sidebranch, resulting in a shift in excitation of the higher-order branch-mode at higher frequency and thus an increase in the sound transmission of the fundamental mode across the junction along the main duct at the eigen-frequencies of the sidebranch. As the frequency increases, the non-planar branch-mode is excited and thus acoustic power is transmitted into the sidebranch. This causes the decrease in $|T_{00,00}|^2$.

b. Sound-power scattering of the fundamental mode (0,0) into the first mode (1,0), $|T_{00,10}|^2$. Because of acoustic scattering and diffraction at the junction in the main duct, all modes are able to propagate downstream of the junction due to excitation by the fundamental mode and other modes at the entry to the junction at $z=0$. Figure 2(b) shows that the sidebranch acts as a low-pass filter for sound scattering of the fundamental mode into the first duct mode of the x-axis $|T_{00,10}|^2$ at frequencies of $kL_x=\pi$ to 2π. The first mode of the x-axis is able to propagate through the duct at frequencies above $k_{mn=(1,0)}=\pi/L_x$. Generally, $|T_{00,10}|^2$ shows a gradual decrease with increasing frequency from $k_{mn=(1,0)}$. Again, a slight fluctuation in $|T_{00,10}|^2$ at frequencies just above $k_{mn=(1,0)}$ can be caused by the strong evanescent waves at and close to the eigen-frequencies. For $k<L_x/w$, an increase in $|T_{00,10}|^2$ is observed with increasing w/L_x, as shown in Fig. 2(b) with $w/L_x=0.5$ (cf. $w/L_x=0.3$). $|T_{00,10}|^2$ vanishes at the eigen-frequency of the (2,0) duct mode, $k=2\pi/L_x$.

Figure 4 shows the sound-pressure field due to fundamental-mode excitation with small $w/L_x(=0.5)$. A high sound pressure occurs inside the junction at $x=0$ at frequencies above and close to $k_{mn=(1,0)}$ [Fig. 4(a)]. With increasing frequency, the region of high sound pressure is extended to the exit of the junction, and the strength is reduced [Fig. 4(b)]. Sound pressure is again high inside the junction at the frequency close to $k_{mn=(2,0)}$; however, this area is located close to the center of the junction, as shown in Fig. 4(c). This positioning results in inefficient excitation of the first asym-

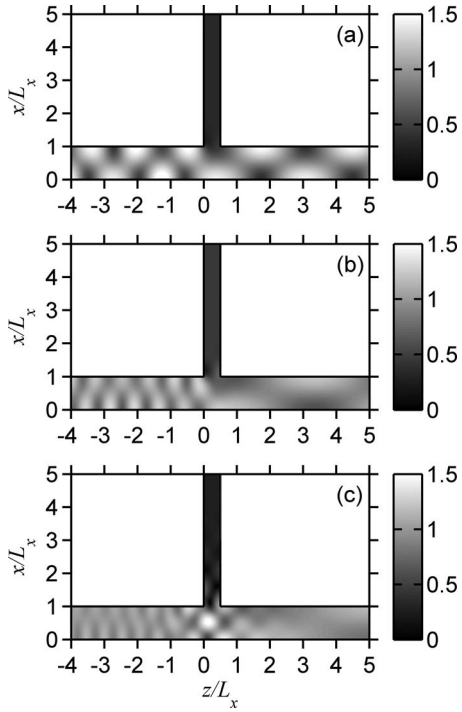

FIG. 4. Sound-pressure field (Pa) around the tee-junction between the main duct and an infinitely long sidebranch with $w/L_x=0.5$ due to fundamental-mode excitation. (a) $kL_x=1.050\pi$, (b) $kL_x=1.500\pi$, and (c) $kL_x=1.950\pi$.

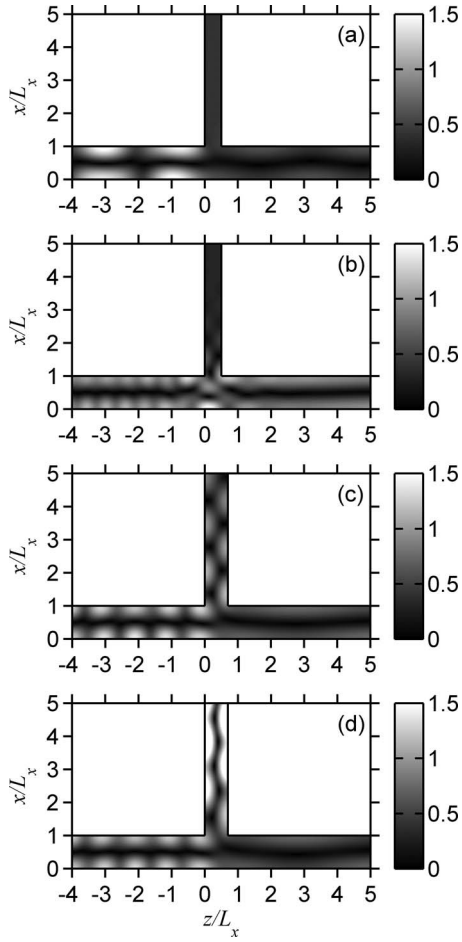

FIG. 5. Sound-pressure field (Pa) around the tee-junction between the main duct and an infinitely long sidebranch due to unit (1,0) mode excitation. (a) $kL_x=1.100\pi$, $w/L_x=0.5$; (b) $kL_x=1.950\pi$, $w/L_x=0.5$; (c) $kL_x=1.429\pi$, $w/L_x=0.7$; (d) $kL_x=1.436\pi$, $w/L_x=0.7$.

metric mode and the vanishing of sound scattered into the $(p,q)=(1,0)$ mode by the fundamental mode downstream of the junction along the main duct at a frequency close to $k_{mn=(2,0)}$. For $k>L_x/w$, a marked drop in $|T_{00,10}|^2$ occurs as frequency increases from $k_{mn=(1,0)}$ to the eigen-frequencies of the sidebranch. $|T_{00,10}|^2$ reaches a local minimum at or close to the eigen-frequencies of the sidebranch ($k=\alpha L_x/w$). Figures 2(a) and 2(b) shows weak modal coupling of the branch-mode and traveling wave in the junction at or close to the eigen-frequencies of the sidebranch, as a consequence of high $|T_{00,00}|^2$ and low $|T_{00,10}|^2$. The sudden fall in $|T_{00,00}|^2$ [Fig. 2(a)] at the frequency slightly above the eigen-frequencies of the sidebranch results in a small jump in $|T_{00,10}|^2$ [Fig. 2(b)] due to the non-uniform distribution of pressure at the exit of the tee-junction along the main duct; thus, some acoustic power is scattered into the (1,0) mode [Fig. 3(c)], followed by minor fluctuations with increasing frequency. For large w/L_x, a more effective scattering of the fundamental mode into the (1,0) mode can be observed at frequencies above $k=L_x/w$ [Fig. 2(b)], with excitation of the non-planar branch-mode and thus non-uniform distribution of pressure at $z=w$.

c. Sound-power transmission of the first mode (1,0), $|T_{10,10}|^2$. Similar to the situation for $|T_{00,00}|^2$ at frequencies below $k_{mn=(1,0)}$,[3] the tee-junction acts as a high-pass filter for the sound-power transmission of the first duct mode $|T_{10,10}|^2$ at frequencies between $k_{mn=(1,0)}=\pi/L_x$ and $k_{mn=(2,0)}=2\pi/L_x$ of the x-axis modes, as shown in Fig. 2(c); however, the vanishing of $|T_{10,10}|^2$ can be observed at or close to $k_{mn=(1,0)}$. Again, a fluctuation in $|T_{10,10}|^2$ at frequencies just above the eigen-frequency of the main duct $k_{mn=(1,0)}$ occurs due to the strong evanescent waves. Sound transmission of the (1,0) mode, $|T_{10,10}|^2$, becomes increasingly effective with increasing frequency, approaching $k_{mn=(2,0)}$. A rapid increase in $|T_{10,10}|^2$ occurs with increasing frequency from $k_{mn=(1,0)}$, and sound transmission of the (1,0) mode becomes more effective with decreasing w/L_x because less acoustic power is taken away by the sidebranch. For frequencies below $k=L_x/w$, $|T_{10,10}|^2$ approaches unity at $k_{mn=(2,0)}$, which is an eigen-frequency of the higher-order x-axis mode. Again, a sharp fall in $|T_{10,10}|^2$ is followed by fluctuating values at frequencies just above the eigen-frequencies of the sidebranch [e.g., Fig. 2(c) with $w/L_x=0.7$, 1.5, and 2.0].

Figure 5 shows the sound-pressure field around the tee-junction arising from excitation of the (1,0) mode only in the area upstream of the duct. A strong standing wave of the first mode (1,0) is observed upstream of the duct [Fig. 5(a)], indicating the occurrence of high modal reflection at frequencies close to that of the (1,0) mode. With increasing frequency, high sound pressure occurs inside the junction at $x=0$; thus, effective transmission of the (1,0) mode is observed close to $k_{mn=(2,0)}$ [Fig. 5(b)]. Again, the non-planar branch-mode is suppressed at or close to the eigen-frequencies of the sidebranch [Fig. 5(c)] because of weak coupling of the branch-mode and traveling wave in the junction. With increasing frequency, a sudden drop in $|T_{10,10}|^2$

occurs in response to the improved distribution of acoustic velocity at the entry to the sidebranch (data not shown). Strong resonance of the branch-mode is observed at frequencies slightly higher than the eigen-frequencies of the sidebranch [Fig. 5(d)]; however, the effects of the non-planar branch-mode on the sound transmission of higher-order modes are reduced compared with the effects on fundamental-mode transmission, especially for higher-order branch-modes [Fig. 2(c)]. The scattering of other modes is minor, and is not considered here.

d. Discussion of infinitely long sidebranch. In general, sound transmissions of fundamental mode and higher-order modes are high at the eigen-frequencies of the main duct and branch. These are due to resonance of the main duct and weak modal coupling between the branch-mode and traveling wave in the junction, respectively. With the excitation of the non-planar branch-mode, a decrease in sound transmission can be observed. A fluctuation in sound transmission and scattering at frequencies just above the eigen-frequencies of the main duct occurs due to the strong evanescent waves.

2. Branch-end reflection

Two types of longitudinal branch resonance have been found to be critical for the sound transmission of fundamental mode at frequencies below $k_{mn=(1,0)}$ due to the end reflection of the sidebranch:[3] the "both-ends-closed" and "one-end-closed–one-end-open" types, which correspond to the creation of high and low pressures at the entry to the sidebranch, respectively. Moreover, $|T_{00,00}|^2$ approaches zero and unity for infinitely long and closed sidebranches, respectively, at very low frequency, $kd \to 0$. Here, we investigate the case of a closed sidebranch using numerical experiments, and the frequency is extended to the higher-order modes of the x-axis, $k_{mn=(2,0)}$. We consider the effects of two types of longitudinal branch resonance and non-planar branch-modes on sound transmission in higher-order modes.

Figures 6(a)–6(d) show the sound-power transmission of a fundamental mode $|T_{00,00}|^2$ and sound-power scattering of a fundamental mode into the (1,0) mode $|T_{00,10}|^2$, respectively, for a duct across a 1-m-long closed sidebranch along the main duct at various high frequencies between $kL_x = \pi$ and 2π. $|T_{00,00}|^2$ attains minima at certain frequencies in response to the two types of branch resonances. These two types of branch resonance are excitation of the longitudinal branch resonance in a low-pressure region created at the entry to the sidebranch at frequencies $1.4\pi < kL_x < 1.6\pi$ and excitation of the non-planar branch-mode.

Figure 7(a) shows the sound-pressure field at the minimum point in Fig. 6(a) with $w/L_x = 0.3$, due to a one-end-closed–one-end-open type of longitudinal branch resonance at frequencies above $k_{mn=(1,0)}$. A low-pressure region is created inside the junction and at the entry to the sidebranch, while a high-pressure region is created in the wall opposite the sidebranch. This non-uniform distribution of sound pressure results in effective scattering of the fundamental mode into the asymmetric mode (1,0) downstream of the junction, along the main duct [Figs. 6(c) and 7(a)]. In addition to an increase in w/L_x, more inclined nodal and anti-nodal planes

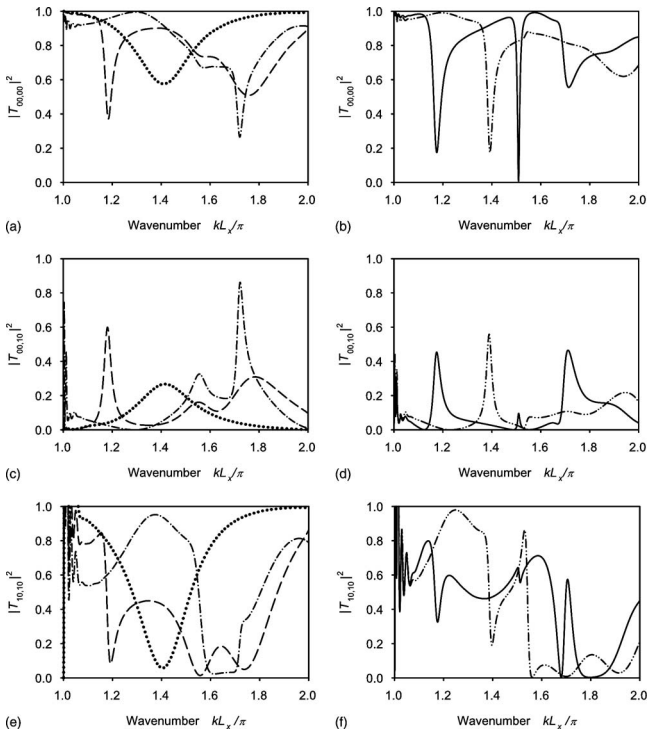

FIG. 6. Sound-power transmission and scattering across a closed sidebranch along the main duct. $l/L_x = 1$. [(a) and (b)] $|T_{00,00}|^2$, [(c) and (d)] $|T_{00,10}|^2$, and [(e) and (f)] $|T_{10,10}|^2$. (·····) $w/L_x = 0.3$; (– – – –) $w/L_x = 0.9$; (–·–·–) $w/L_x = 1.2$; (–··–··–) $w/L_x = 1.5$; (—) $w/L_x = 1.8$.

are observed [Fig. 7(b)]. The inclined nodal plane at the entry to the sidebranch extends to the center of the junction, and the high-pressure region in the wall opposite the sidebranch is reduced in size. These changes lead to an increase in the effectiveness of sound transmission of the fundamental mode $|T_{00,00}|^2$ and a reduction in the effectiveness of sound

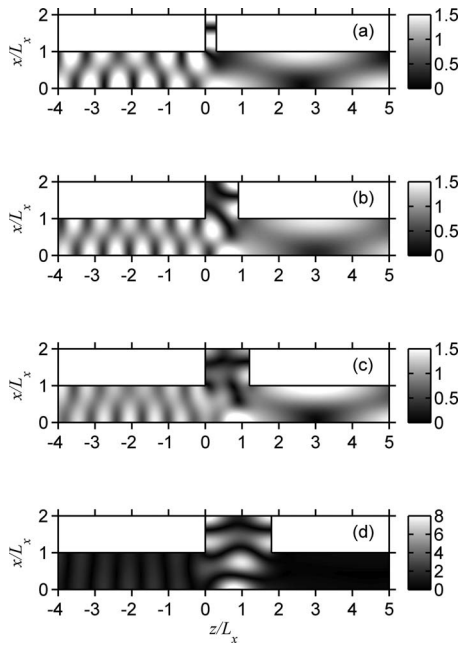

FIG. 7. Sound-pressure field (Pa) around the tee-junction between the main duct and a closed sidebranch due to fundamental-mode excitation, with $l/L_x = 1$. (a) $kL_x = 1.410\pi$; $w/L_x = 0.3$; (b) $kL_x = 1.552\pi$; $w/L_x = 0.9$; (c) $kL_x = 1.556\pi$, $w/L_x = 1.2$; (d) $kL_x = 1.510\pi$, $w/L_x = 1.8$.

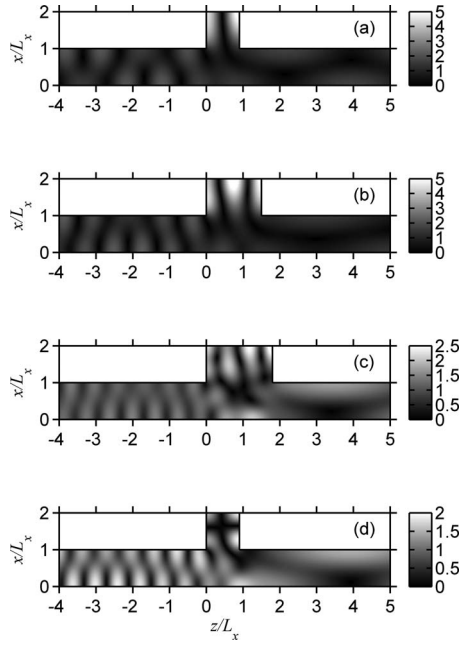

FIG. 8. Sound-pressure field (Pa) around the tee-junction between the main duct and a closed sidebranch due to fundamental-mode excitation, with $l/L_x=1$. (a) $kL_x=1.184\pi$, $w/L_x=0.9$; (b) $kL_x=1.392\pi$, $w/L_x=1.5$; (c) $kL_x=1.714\pi$, $w/L_x=1.8$; (d) $kL_x=1.756\pi$, $w/L_x=0.9$.

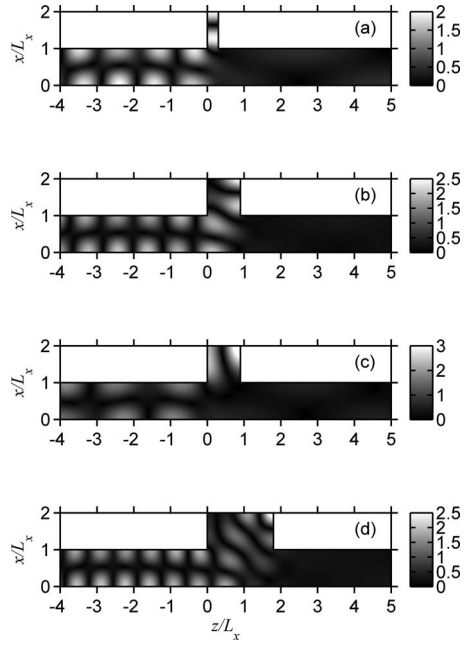

FIG. 9. Sound-pressure field (Pa) around the tee-junction between the main duct and a closed sidebranch due to unit (1,0) mode excitation, with $l/L_x=1$. (a) $kL_x=1.404\pi$, $w/L_x=0.3$; (b) $kL_x=1.558\pi$, $w/L_x=0.9$; (c) $kL_x=1.192\pi$, $w/L_x=0.9$; (d) $kL_x=1.796\pi$, $w/L_x=1.8$.

scattering into the first asymmetric mode $|T_{00,10}|^2$ downstream of the junction. The inclined nodal and anti-nodal planes also act to shift the frequency of the minimum points of $|T_{00,00}|^2$ toward the higher side with increasing w/L_x, e.g., the plot for $w/L_x=0.3$ and 0.9 in Figs. 6(a), 7(a), and 7(b). For large w/L_x, the co-excitation of the non-planar and longitudinal branch-modes results in a decrease in $|T_{00,00}|^2$ [Fig. 7(c) with $w/L_x=1.2$].

A more effective scattering of the fundamental mode into the first asymmetric duct mode $|T_{00,10}|^2$ is observed with excitation of the non-planar branch-mode, as shown in Figs. 6(c) and 7(c). Figures 7(a) and 7(b) show the inclined nodal plane (low-pressure region) at the entry to the sidebranch at higher frequencies but with the same l/L_x, for which the longitudinal branch resonance is subdued and $|T_{00,00}|^2$ does not vanish at frequencies higher than $k_{mn=(1,0)}$, in contrast to the vanishing observed at low frequencies (see Fig. 8 in Ref. 3). The excitation of strong resonance of longitudinal branch-modes results in vanishing $|T_{00,00}|^2$ and a reduction in the frequency of the minimum point [Fig. 7(d)]. The non-planar mode is suppressed because of the weak modal coupling of the non-planar branch-mode and the traveling wave at or close to the eigen-frequencies of the sidebranch. The development of a strong standing wave in the duct upstream of the junction and inside the sidebranch indicates the high reflection of sound and strong longitudinal branch resonance. There exists a uniform distribution of acoustic velocity (upward) at the entry to the sidebranch (data not shown), and $|T_{00,00}|^2$ and $|T_{00,10}|^2$ are low, as shown in Figs. 6(b) and 6(d). Scattering is less dependent on excitation of the longitudinal branch-mode [Figs. 6(c) and 6(d) at a frequency of $1.4\pi < kL_x < 1.6\pi$]. The minima in Figs. 6(a) and 6(b) outside the range of $1.4\pi < kL_x < 1.6\pi$ are caused by excitation of the non-planar branch-modes (e.g., Fig. 8); however, sound transmission does not completely vanish at higher frequencies [compare with the results reported by Tang[3] at frequencies below $k_{mn=(1,0)}$]. For excitation of the second branch-mode at frequencies of $kL_x=1.722\pi$, 1.392π, and 1.176π with $w/L_x=1.2$, 1.5, and 1.8, respectively, we observed that the eigen-frequencies of the sidebranch are shifted toward the high side, and $|T_{00,00}|^2$ decreases with increasing w/L_x, as shown in Figs. 6(a) and 6(b). Again, a strong scattering of the fundamental mode into the first asymmetric mode $|T_{00,10}|^2$ is observed with excitation of the non-planar branch-mode [Figs. 8(a)–8(c)]. In the case of co-excitation of the longitudinal branch-mode and non-planar branch-mode, we find a more broad band-stop action in $|T_{00,00}|^2$ [Figs. 6(a) and 8(d)].

Figures 6(e) and 6(f) show the effects of w/L_x on the sound-power transmission of the (1,0) mode $|T_{10,10}|^2$ across the junction and along the main duct at various frequencies between $k_{mn=(1,0)}$ and $k_{mn=(2,0)}$. Vanishing and minimum $|T_{10,10}|^2$ are found with excitation of the longitudinal branch-modes within the low-pressure region at the entry to the sidebranch and with excitation of non-planar branch-modes.

Figures 9(a) and 9(b) shows the sound-pressure fields at frequencies of vanishing $|T_{10,10}|^2$ due to the excitation of one-end-closed–one-end-open type of longitudinal branch resonance in the range $1.4\pi < kL_x < 1.6\pi$, which is similar to $|T_{00,00}|^2$ [cf. Figs. 7(a) and 7(b)]. Figures 9(c) and 9(d) show excitation of non-planar branch-modes at frequencies of a minimum and vanishing $|T_{10,10}|^2$, respectively, for the case of a closed sidebranch, which yields similar results to that in the case of $|T_{00,00}|^2$ [cf. Figs. 8(a) and 8(c)]. The both-ends-closed type of longitudinal branch resonance, which leads to a high-pressure region at the entry to the sidebranch, results in high $|T_{00,00}|^2$ and $|T_{10,10}|^2$ (data not shown).

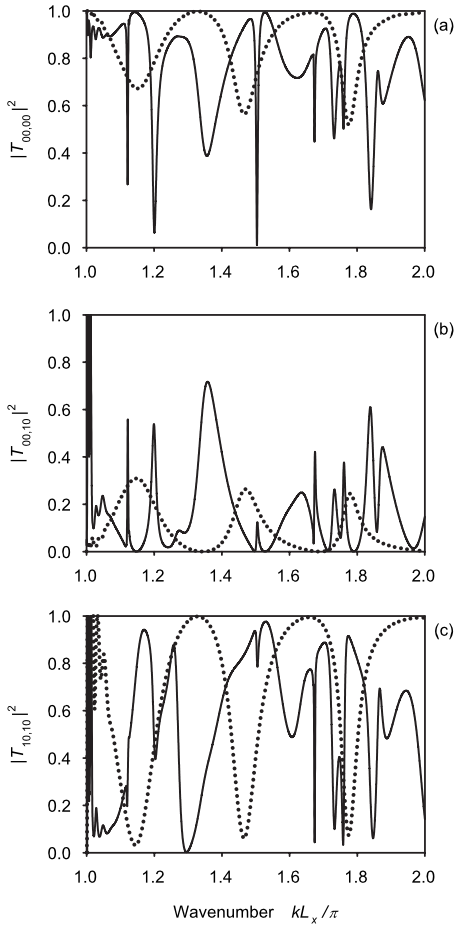

FIG. 10. Sound-power transmission and scattering across a closed sidebranch along the main duct, with $l/L_x=3$. (a) $|T_{00,00}|^2$, (b) $|T_{00,10}|^2$, and (c) $|T_{10,10}|^2$. (·····) $w/L_x=0.3$; (—) $w/L_x=1.8$.

With increasing sidebranch length, additional occurrences of branch resonance are observed; an example for $l/L_x=3$ with $w/L_x=0.3$ and 1.8 is shown in Fig. 10, involving the same mechanism as that described for $l/L_x=1$. The corresponding results are not discussed here.

To summarize this sub-section, the sound transmissions $|T_{00,00}|^2$ and $|T_{10,10}|^2$ are low with excitation of the non-planar branch-mode and excitation of the longitudinal branch resonance when a low-pressure region created at the entry to the sidebranch. However, an increase in $|T_{00,10}|^2$ occurs with excitation of the non-planar branch-mode.

B. Experimental results

Here, the formulations in Sec. II B are used for modal decomposition of the sound-pressure field upstream and downstream of the junction in the test rig within three-dimensional space. Figure 11 shows the sound-power transmission and scattering of fundamental mode with an anechoic sidebranch. Also plotted for comparison are the results of finite element modeling for $|T_{00,00}|^2$, $|T_{00,10}|^2$, and $|T_{10,10}|^2$. In terms of sound transmission and scattering, the results of the experiment show a reasonable match with the results of numerical modeling with anechoic termination at the end of the sidebranch. The sound transmission of fundamental mode, $|T_{00,00}|^2$, shows peaks close to the eigen-

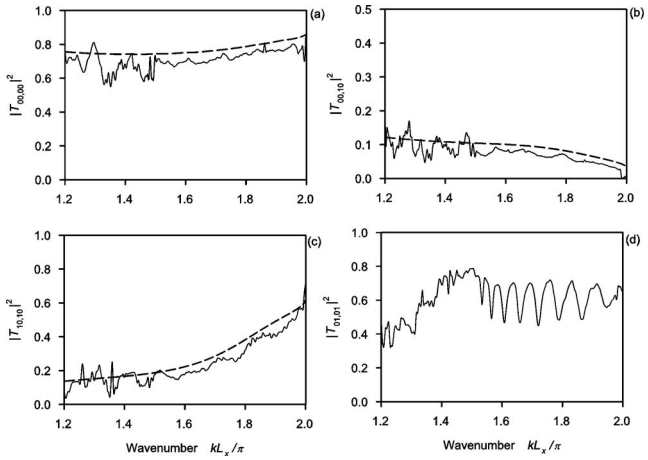

FIG. 11. Sound-power transmission and scattering across a tee-junction with anechoic termination along the main duct. (a) $|T_{00,00}|^2$, (b) $|T_{00,10}|^2$, (c) $|T_{10,10}|^2$, and (d) $|T_{01,01}|^2$. (—) measured data; (– – – – –) simulation results.

frequencies of the x-axis mode, $k_{mn=(m,0)}$ [Fig. 11(a)]. High sound scattering of the fundamental mode to the first mode $|T_{00,10}|^2$ is observed close to $k_{mn=(1,0)}$, although a gradual decrease is observed with increasing frequency [Fig. 11(b)]. As mentioned above, $|T_{00,10}|^2$ attains a minimum at the (2,0) mode, $k=2\pi/L_x$.

The experiment reveals a dramatic fluctuation in the results at frequencies close to the eigen-frequencies of the duct at $kL_x=\pi$ to 1.2π, reflecting the influence of the evanescent mode; therefore, those results are not shown here. For sound transmission of the first mode across the junction, $|T_{10,10}|^2$ shows a vanishing trend at $k_{mn=(1,0)}$. With increasing frequency, sound transmission of the first mode becomes increasingly effective, as shown in Fig. 11(c). Figure 11(d) shows the sound transmission of the first mode of the y-axis $|T_{01,01}|^2$, a scenario that cannot be evaluated using the two-dimensional numerical experiments described in Sec. III A. The upward trend in $|T_{01,01}|^2$ observed at frequencies from $k_{mn=(0,1)}$ to $k_{mn=(1,1)}$ [Fig. 11(d)] is similar to that of $|T_{00,00}|^2$ from $k_{mn=(0,0)}$ to $k_{mn=(1,0)}$ [i.e., from $k=0$ to π/L_x], as shown in Fig. 2 in Ref 3. This finding indicates the same mechanism of sound transmission for the non-planar mode of the y-axis as that for the fundamental mode. The fluctuation of $|T_{01,01}|^2$ at frequencies above the eigen-frequency of the (1,1) mode at $kL_x=1.53\pi$ is due to modal coupling of the spanwise branch-mode and the traveling wave at the junction.[16]

Figure 12 shows $|T_{00,00}|^2$, $|T_{00,10}|^2$, $|T_{10,10}|^2$, and $|T_{01,01}|^2$ with a 1-m-long closed sidebranch. The finite element model slightly overestimates the sound transmission and scattering compared with measured values, especially for cases of sound transmission for higher-order modes. This discrepancy possibly reflects the occurrence of modal damping within the duct, especially at high frequencies; however, the results are with acceptable engineering tolerance.

As mentioned above, the minima in $|T_{00,00}|^2$ and $|T_{10,10}|^2$ are found in response to excitation of the branch resonances, as shown in Figs. 12(a) and 12(c). The modal decomposition method can satisfactorily solve the modal transmission and scattering coefficients. Figure 12(d) indicates several minima in $|T_{01,01}|^2$ at some frequencies between $kL_x=1.5\pi$ and 2π.

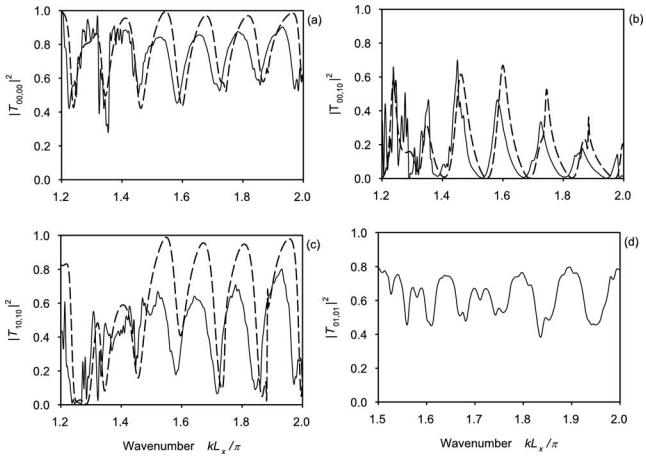

FIG. 12. Sound-power transmission and scattering across a 1-m-long closed tee-junction along the main duct. (a) $|T_{00,00}|^2$, (b) $|T_{00,10}|^2$, (c) $|T_{10,10}|^2$, and (d) $|T_{01,01}|^2$. (—) measured data; (– – – – –) simulation results.

The fluctuation in $|T_{01,01}|^2$ at higher frequencies is possibly due to branch resonances. High sound transmission of the higher-order modes is observed in Figs. 11(c), 11(d), 12(c), and 12(d), thereby confirming the importance of sound propagation at higher-order modes.

Figures 13(a) and 13(b) shows the sound scattering of the (0,1) mode into the (1,1) mode and sound transmission of the (1,1) mode across the junction with an anechoic termination, respectively, revealing downward and upward trends. Fluctuations are due to modal coupling of the spanwise branch-mode and the traveling wave in the duct. Again, Figs. 11(b) and 13(a) reveal high sound scattering into higher-order modes at the frequency of the transmitted higher-order modes. Figures 11(c) and 13(b) demonstrate that sound transmission of high-order modes and the fundamental mode (as shown in Ref. 3) is increased from its eigen-frequency to a higher eigen-frequency. Finally, Figs. 13(c) and 13(d) show

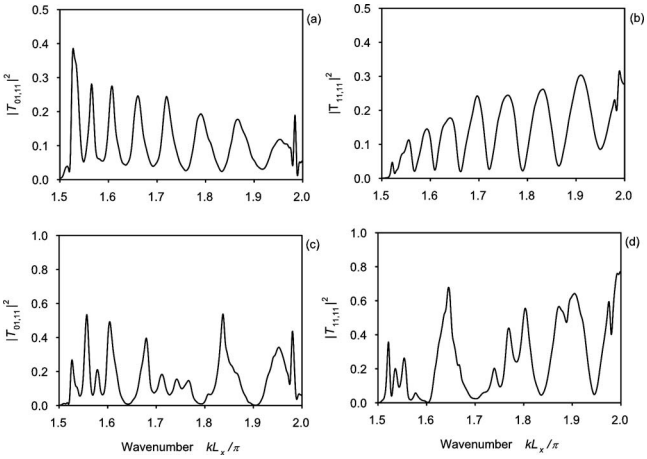

FIG. 13. Experimental results of sound-power transmission and scattering across a 1-m-long closed tee-junction along the main duct. [(a) and (b)] $|T_{01,11}|^2$ and $|T_{11,11}|^2$ across a tee-junction with anechoic termination along the main duct, respectively; [(c) and (d)] $|T_{01,11}|^2$ and $|T_{11,11}|^2$ across a 1-m-long closed tee-junction along the main duct, respectively. (—) measured data; (– – – – –) simulation results.

that high sound scattering and transmission (with end reflection of the sidebranch) can be observed at higher frequencies in higher-order modes.

The numerical results in Sec. III A are verified in this sub-section using direct modal decomposition method. The experimental method for measurement of sound transmission and scattering of rectangular duct in higher-order modes is demonstrated. There exists a difficulty in the measurement at frequencies close to the eigen-frequency of the main duct due to the strong evanescent waves. For the tests with branch-end reflection, the measured values are slightly less than that of the numerical simulations due to the occurrence of modal damping in the experiments.

IV. CONCLUSIONS

We investigated the sound-transmission characteristics of a tee-junction along an infinitely long rectangular duct using numerical simulations and model experiments. The analysis considered infinitely long sidebranches and closed sidebranches. Sound transmission and scattering of the first four acoustic modes across the tee-junction of the duct were decomposed and investigated experimentally.

For an infinitely long sidebranch, two acoustical multi-band filters in series can be observed in the sound transmission of fundamental mode. The tee-junction acts as a multi-band filter for the fundamental mode. The pass-bands of the filter are found at the eigen-frequencies of the axial mode in the axis along the sidebranch, along which the sound transmission of fundamental mode gradually increases from a very low frequency and approaches a maximum at the eigen-frequencies of the axial mode of the main duct. An increase in sidebranch width results in higher attenuation at the stop-bands of the filter as the sidebranch takes away larger amounts of acoustic power. Another relevant mechanism is the weak coupling of the branch-mode and traveling wave in the junction at the entry to the sidebranch, which provides multi-band filtering with pass-bands at or very close to the eigen-frequencies of the sidebranch, thereby shifting excitation of the higher-order non-planar branch-modes at higher frequency. Sound transmission decreased with excitation of the non-planar branch-mode; however, this effect is reduced for sound transmission of higher-order modes across the junction along the main duct because of weaker coupling of the branch-modes and traveling wave in the junction. Sound transmission of the axial mode along the sidebranch axis vanishes at its eigen-frequencies and increases as the frequency approaches the eigen-frequency of the immediately higher axial mode along the same axis of the sidebranch. For sound scattering into higher acoustic modes, the sidebranch acts as a low pass filter; for example, sound scattering from fundamental mode into the first asymmetric mode of the duct in the axis along the sidebranch becomes more effective as the frequency approaches the eigen-frequency of the first asymmetric mode; it also decreases with increasing frequency. Sound scattering into higher-order modes is increased with excitation of the non-planar branch-mode, and

an increase in sidebranch width results in an increase in sound scattering and the reduced transmission of higher-order modes.

In the case of a closed sidebranch, lower sound transmission of higher-order modes are observed with excitation of the longitudinal branch-mode in the low-pressure region created at the entry to the sidebranch and with excitation of the non-planar branch-mode. The inclined nodal plane of the longitudinal branch-mode means that sound transmission does not vanish at higher frequencies; however, vanishing of the sound transmission of fundamental mode and a reduction in the effectiveness of higher-order-mode scattering are observed for a strong standing wave of the longitudinal branch-mode and suppression of the non-planar branch-mode.

A procedure of measurement of sound transmission and scattering of a duct element in a rectangular duct is reported, using a modal decomposition approach based on the transfer functions of microphones located at different axial positions. Further simplification of the formulation is possible if the modal reflection condition is known downstream of the duct termination. The present study experimentally verified the sound-transmission coefficients of a tee-junction. The experiment results are reasonably consistent with the simulation results; however, the simulation of a tee-junction with branch-end reflection and a hard-wall overestimated the sound transmission and scattering, possibly due to modal damping at high frequencies. Fluctuations in sound transmission and scattering are observed due to coupling of the spanwise branch-mode and traveling wave.

The sound-transmission characteristics of a tee-junction at higher-order mode have been shown. Such problems frequently arise when the sound propagation in waveguide is at frequencies higher than first eigen-frequency of the duct. Ventilation duct is a representative example. A procedure of the measurement of sound transmission of scattering at higher-order mode is demonstrated in the present study.

ACKNOWLEDGMENTS

This work was fully supported by a grant from the Hong Kong Polytechnic University (Project A/C No. G-U362). We would like to thank Professor S. K. Tang (Department of Building Services Engineering, The Hong Kong Polytechnic University) for support with finite element computations and for valuable advice.

[1]A. Cummings, "Sound transmission in curved duct bends," J. Sound Vib. **35**, 451–477 (1974).
[2]S. K. Tang and F. Y. C. Li, "On low frequency sound transmission loss of double sidebranches: A comparison between theory and experiment," J. Acoust. Soc. Am. **113**, 3215–3225 (2003).
[3]S. K. Tang, "Sound transmission characteristics of tee-junctions and the associated length corrections," J. Acoust. Soc. Am. **115**, 218–227 (2004).
[4]S. K. Tang and C. K. Lau, "Sound transmission across a smooth nonuniform section in an infinitely long duct," J. Acoust. Soc. Am. **112**, 2602–2611 (2002).
[5]C. K. Lau and S. K. Tang, "Sound transmission across duct constrictions with and without tapered sections," J. Acoust. Soc. Am. **117**, 3679–3685 (2005).
[6]D. D. Reynolds and J. M. Bledsoe, *Algorithms for HVAC Acoustics* (American Society of Heating, Refrigerating and Air-Conditioning Engineers, Atlanta, GA, 1991).
[7]*ASHRAE Handbook—Applications* (American Society of Heating, Refrigerating and Air-Conditioning Engineers, Atlanta, GA, 2007).
[8]J. L. Parrondo, J. Fernández, I. García, and E. Ruiz, "Noise transmission through duct divisions in air circuits, considered as three-port acoustic systems," J. Sound Vib. **296**, 183–194 (2006).
[9]*ASHRAE Handbook—Fundamentals* (American Society of Heating, Refrigerating and Air-Conditioning Engineers, Atlanta, GA, 2005).
[10]J. Y. Kwon, H. H. Park, and H. J. Eom, "Acoustic scattering from two junctions in a rectangular waveguide," J. Acoust. Soc. Am. **103**, 1209–1212 (1998).
[11]J. Y. Kwon and H. J. Eom, "Acoustic hybrid junction in a rectangular waveguide," J. Acoust. Soc. Am. **107**, 1868–1873 (2000).
[12]C. J. Moore, "Measurement of radial and circumferential modes in annular and circular fan ducts," J. Sound Vib. **62**, 235–256 (1979).
[13]M. Abom, "Modal decomposition in ducts based on transfer function measurements between microphone pairs," J. Sound Vib. **135**, 95–114 (1989).
[14]A. Sitel, J. M. Ville, and F. Foucart, "Multiload procedure to measure the acoustic scattering matrix of a duct discontinuity for higher order mode propagation conditions," J. Acoust. Soc. Am. **120**, 2478–2490 (2006).
[15]T. Schultz, L. N. Cattafesta III, and M. Sheplak, "Modal decomposition method for acoustic impedance testing in square ducts," J. Acoust. Soc. Am. **120**, 3750–3758 (2006).
[16]T. C. Redmore and K. A. Mulholland, "The application of mode coupling theory to the transmission of sound in the sidebranch of a rectangular duct system," J. Sound Vib. **85**, 323–331 (1982).
[17]V. Pagneux, N. Amir, and J. Kergomard, "A study of wave propagation in varying cross-section waveguides by modal decomposition. I. Theory," J. Acoust. Soc. Am. **100**, 2034–2048 (1996).
[18]M. L. Munjal, *Acoustics of Ducts and Mufflers with Application to Exhaust and Ventilation System Design* (Wiley, New York, 1987).
[19]*ASHRAE Handbook—HVAC Applications* (American Society of Heating, Refrigerating and Air-Conditioning Engineers, Atlanta, GA, 2007).